Stable quadratic solitons consisting of fundamental waves and oscillatory second harmonics subject to boundary confinement

Jing Wang,* Zhenlei Ma, Yiheng Li, Daquan Lu, Qi Guo, and Wei Hu†

Guangdong Provincial Key Laboratory of Nanophotonic Functional Materials and Devices, South China Normal University, Guangzhou 510006, People's Republic of China

(Received 12 December 2014; published 2 March 2015)

We investigate quadratic solitons consisting of fundamental waves and oscillatory second harmonics, which can be stable when subject to boundary confinement. A family of quadratic solitons whose fundamental waves can be monopole, dipole, or even multipole are found numerically. The existence of solitons, depending on the sample size and degree of nonlocality, are given for strongly, generally, and weakly nonlocal cases, respectively.

DOI: 10.1103/PhysRevA.91.033801 PACS number(s): 42.65.Tg, 42.65.Jx, 42.65.Ky, 42.65.Sf

I. INTRODUCTION

Quadratic solitons, a type of parametric soliton supported by quadratic nonlinearities, consist of coupled and mutually trapped two-frequency waves [1,2]. The trapping results from the rapid exchange of phase and energy between the two-frequency waves rather than the self-induced change in the refractive index. Since their theoretical prediction [3,4] in the 1970s and experimental observations [5,6] in the 1990s, quadratic solitons have attracted increasing attention because of their potential applications in ultrafast all-optical switching and controlling of light by light [7,8]. To date, the basic properties of quadratic solitons have been well investigated [2,9], and the underlying physics behind them have also been discovered by several authors [10,11].

On the other hand, nonlocal solitons, solitons in nonlinear media with a nonlocal response, have also been studied extensively in the recent past [12–16]. In the nonlocal response in nonlinear media, the refractive index change at a given point is determined not only by the light intensity at that point but also by the light intensity near that point. There are several types of nonlocal response in real nonlinear media, such as the zeroth-order modified Bessel nonlocal response in nematic liquid crystals [13], the logarithmic nonlocal response in lead glass [17], and the exponential-decay-type nonlocal response in aqueous solution of rhodamine B [18] and diluted India ink [19].

Nikolov *et al.* found that quadratic solitons are equivalent to nonlocal solitons on the basis of an analogy between parametric interaction and diffusive nonlocality [20]. The nonlocal analogy was later used to successfully describe pulse compression [21,22], localized X waves [23], and modulational instability [24] in $\chi^{(2)}$ materials. Nikolov *et al.* showed that the second harmonic (SH), like the nonlinear refractive index forming a waveguide, traps the fundamental wave (FW). They found two types of response functions, the exponential-decay type and the sine-oscillatory type. On the basis of the sine-oscillatory-type response function, one can understand why Buryak and Kivshar found numerically that quadratic solitons radiate linear waves [20,25]. In 2012, Esbensen *et al.* further investigated quadratic solitons with a sine-oscillatory type response function and found a family of analytical solutions under the strongly nonlocal approximation [26]. However, these soliton solutions, whether numerical or analytical, were all unstable. We have shown that boundary conditions can stabilize this type of nonlocal soliton with sine-oscillatory response functions [27].

In this paper, we further investigated these oscillatory quadratic solitons. We found a family of quadratic solitons consisting of monopole, dipole, or even multipole FWs and oscillatory SHs. We analyzed the existence of these solitons by numerical simulation for strongly, generally, and weakly nonlocal cases, respectively. We found that the existence of the solitons depends on the sample size and degree of nonlocality.

II. NONLOCAL MODEL

We start our analysis by considering an FW and its SH propagating along the z direction in a lossless quadratic nonlinear medium under conditions for type-I phase matching. The evolution of their slowly varying envelopes E_1 and E_2 can be described by the dimensionless dynamical equations [20]

$$i\frac{\partial E_1}{\partial z} + d_1\frac{\partial^2 E_1}{\partial x^2} + E_1^* E_2 e^{-i\beta z} = 0, \tag{1}$$

$$i\frac{\partial E_2}{\partial z} + d_2\frac{\partial^2 E_2}{\partial x^2} + E_1^2 e^{i\beta z} = 0. \tag{2}$$

Here the parameter β represents the dimensionless phase mismatch. In the spatial domain, $d_1 \approx 2d_2$, $d_j > 0\,(j = 1,2)$, and x stands for the transverse spatial coordinate. The terms $\partial^2 E_j/\partial x^2$ then denote the beam diffraction. In the temporal domain, d_j is arbitrary, and x stands for the time coordinate. The terms $\partial^2 E_j/\partial x^2$ then denote the group velocity dispersion.

We search for stationary solutions of Eqs. (1) and (2) in the form $E_1(x,z) = \varphi_1(x)\exp(i\lambda z)$ and $E_2(x,z) = \varphi_2(x)\exp(i2\lambda z + i\beta z)$, where λ is the propagation constant. Substituting in Eqs. (1) and (2), we obtain

$$-\lambda\varphi_1 + d_1\frac{d^2\varphi_1}{dx^2} + \varphi_1\varphi_2 = 0, \tag{3}$$

$$-(2\lambda + \beta)\varphi_2 + d_2\frac{d^2\varphi_2}{dx^2} + \varphi_1^2 = 0. \tag{4}$$

Equations (3) and (4) have four parameters (i.e., d_1, d_2, β, and λ), which seems too complicated. By introducing the

*optica@qq.com
†Corresponding author: huwei@scnu.edu.cn

scaling parameters, $\tau = x|\lambda/d_1|^{1/2}$, $\phi_1 = \varphi_1/\lambda|(2d_1)/d_2|^{1/2}$, $\phi_2 = \varphi_2/\lambda$, $s_j = \mathrm{sgn}(\lambda \mathrm{d_j}) = \pm 1$, $\alpha = (2+\beta/\lambda)|d_1/d_2|$, and $\alpha > 0$, as in Ref.[20,25,26], one can obtain a group of simple equations [25]:

$$s_1 \frac{\partial^2 \phi_1}{\partial \tau^2} - \phi_1 + \phi_1 \phi_2 = 0, \tag{5}$$

$$s_2 \frac{\partial^2 \phi_2}{\partial \tau^2} - \alpha \phi_2 + \frac{1}{2}\phi_1^2 = 0. \tag{6}$$

Here the sign parameter s_1 describes whether the nonlinearity of the system is self-focusing ($s_1 = 1$) or self-defocusing ($s_1 = -1$), whereas s_2 describes whether the response function of the system is the exponential-decay type ($s_2 = 1$) or the sine-oscillatory type ($s_2 = -1$). The soliton solutions of Eqs. (5) and (6) for $s_2 = 1$ can be stable without boundary confinement [3,4,20,25], whereas the soliton solutions for $s_2 = -1$ cannot be stable unless subject to boundary confinement [25–29]. We consider only the case $s_2 = -1$ and $s_1 = 1$ in this paper.

We solved exactly the unbounded Eq. (6) in view of the Fourier transform. As a result, the SH can be expressed with the FW in the form of a convolution [20,26],

$$\phi_2 = \frac{1}{2\alpha} \int_{-\infty}^{\infty} R(\tau - \xi)\phi_1^2(\xi) d\xi, \tag{7}$$

where

$$R(\tau) = \frac{1}{2\sigma} \sin\left(\frac{|\tau|}{\sigma}\right). \tag{8}$$

Here $\sigma = 1/\sqrt{\alpha}$ is a parameter that measures the degree of nonlocality. Equation (7) is a general form of the nonlocal Kerr nonlinearity, provided ϕ_2 is regarded as the nonlinear refractive index. Mutual trapping of an FW with its SH in quadratic nonlinear media is equivalent to self-trapping of an optical wave by its self-induced change in refractive index in a nonlocal Kerr nonlinear medium, which was shown well by Nikolov *et al.* [20]. The unbounded sine-oscillatory response function Eq. (8) satisfies shift invariance and depends on the relative positions of the source point and field point. As shown in Fig. 1(a), the response function oscillates with the period $2\pi\sigma$ and amplitude $1/(2\sigma)$ from the center $\tau = 0$ upward to each side until infinity. Quadratic solitons with this unbounded sine-oscillatory response function are all unstable.

To stabilize the oscillatory quadratic solitons, we imposed on Eqs. (5) and (6) first-type boundary conditions, i.e., $\phi_j(l_1) = \phi_j(l_2) = 0$, where l_j represents the positions of the boundary (we assume $l_2 > l_1$ in this paper). Then we solved Eq. (6) exactly using the Green's function method in the presence of the boundary conditions. The dependence of ϕ_2 on ϕ_1 becomes

$$\phi_2 = \frac{1}{2\alpha} \int_{l_1}^{l_2} R(\tau, \tau')\phi_1^2(\tau') d\tau', \tag{9}$$

where

$$R(\tau, \tau') = \begin{cases} \frac{\sin(\frac{\tau - l_1}{\sigma}) \sin(\frac{\tau' - l_2}{\sigma})}{\sigma \sin(l/\sigma)}, & l_1 \leqslant \tau \leqslant \tau', \\ \frac{\sin(\frac{\tau' - l_1}{\sigma}) \sin(\frac{\tau - l_2}{\sigma})}{\sigma \sin(l/\sigma)}, & \tau' \leqslant \tau \leqslant l_2. \end{cases} \tag{10}$$

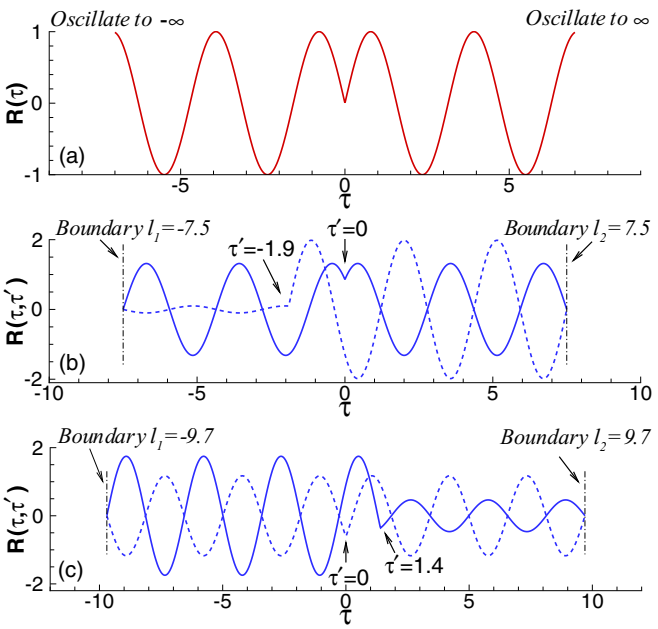

FIG. 1. (Color online) (a) Unbounded sine-oscillatory response function Eq. (8). [(b),(c)] Bounded sine-oscillatory response function Eq. (10). Here $\sigma = 0.5$.

The bounded sine-oscillatory response function Eq. (10) is not shift invariant and depends on the absolute positions of the source point and field point. As shown in Figs. 1(b) and 1(c), the response function oscillates from each boundary point $\tau = l_j$ to the source point $\tau = \tau'$. On each side of the source point sine functions are with the same period $2\pi\sigma$ and different amplitudes. Their derivative $\partial R/\partial\tau$ at the boundary point can be positive or negative, and their phase can be changed to ensure that the source point turns sharply downward. The derivative $\partial R/\partial\tau$ at the source point is discontinuous and is always negative on the left and positive on the right.

III. SOLITON SOLUTIONS

We solved Eqs. (5) and (6) numerically using a Newton iterative scheme in the presence of first-type boundary conditions with $s_2 = -1$ and $s_1 = 1$. We found many quadratic solitons for different sample sizes $l = l_2 - l_1$ and different degrees of nonlocality α. Here the FWs have monopole, dipole, or even multipole profiles, and the profiles of the SHs are oscillatory with a period $T_s = 2\pi\sigma = 2\pi/\sqrt{\alpha}$. According to the size of the soliton width w (defined as $w^2 = 4[\int_{l_1}^{l_2} \tau^2\phi_1^2 d\tau/P - (\int_{l_1}^{l_2} \tau\phi_1^2 d\tau/P)^2]$) for monopole FWs relative to the oscillatory period T_s for oscillatory SHs, the quadratic solitons can be classified into strongly, generally, and weakly nonlocal solitons, corresponding to the different parts in the α domain. Because the soliton width w obtained numerically is on the order of $O(1)$, we define $T_s >> 1$ and $T_s << 1$ as the conditions for strong and weak nonlocality, respectively. Due to the dramatically changing of soliton power P (defined as $P = \int_{l_1}^{l_2} \phi_1^2 d\tau$) for monopole FWs, which can not be shown clearly in a single figure, we show the solutions of solitons in three cases, respectively.

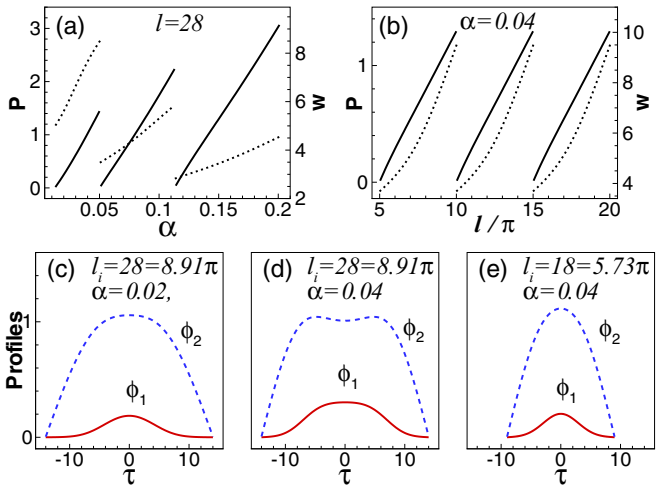

FIG. 2. (Color online) [(a),(b)] Soliton power P (solid line) and width w (dotted line) for FW vs the degree of nonlocality and sample size, respectively. [(c),(e)] Typical soliton profiles with different α and l_i.

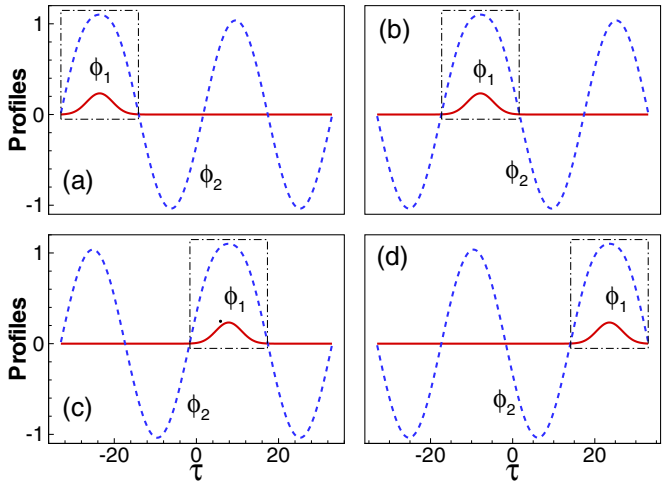

FIG. 3. (Color online) Profiles of solitons when $\alpha = 0.04$ and $l = 66$. Dash-dotted frames represent the ISZ.

A. Strongly nonlocal solutions

In the strongly nonlocal case, the oscillatory period T_s for SHs is always much larger than the soliton width w for FWs. From $T_s >> 1$ we obtain $\alpha << 4\pi^2$. On the basis of the numerical results, we find that $\alpha < 1$ is an acceptable condition for the strongly nonlocal case. Figure 2(a) shows typical curves for the soliton power P and soliton width w for various α values when $l = 28$. The soliton power P and width w for FWs increase piecewise and monotonically with increasing α. Figure 2(b) shows typical P and w curves for various l values when $\alpha = 0.04$ and $T_s = 10\pi$. For any given α, the soliton power P and width w for FWs change piecewise and periodically with a period $T_s/2$ as the sample size l increases. The piecewise properties can be described by the concept of the irreducible soliton zone (ISZ) [27].

We define an ISZ just containing the entire nonzero part of the FW between two zeros of the SH profile. The soliton in the ISZ is called an *irreducible soliton* (IS). The size of the ISZ, l_i, satisfies $T_s/2 < l_i < T_s$. No soliton exists when the sample size is less than $T_s/2$. When the sample is greater than T_s, it can be divided into two parts, the ISZ and several extended zones, as shown in Fig. 3. A soliton in a sample larger than the ISZ can be regarded as an extension of an IS. For the FW, the extension keeps the profiles in the ISZ invariant and pads the zero part in the extended zone. For the SH, the extension keeps the profiles in the ISZ invariant and increases the $m/2$ sine oscillation in the extended zone. A large sample can have one [e.g., Figs. 3(a) and 3(d)] or two [e.g., Figs. 3(b) and 3(c)] extended zones. The total size of the extended zones should be $mT_s/2$ (m is a positive integer). Therefore, one can know all the soliton solutions in the entire sample size l by investigating the IS in the ISZ with a size of l_i using the relation $l = l_i + mT_s/2$.

The relation $l = l_i + mT_s/2$ can explain the curves in Figs. 2(a) and 2(b). In Fig. 2(b), the oscillatory period is $T_s = 10\pi$, and the curves repeat with a period of $T_s/2 = 5\pi$. From the relation $T_s = 2\pi/\sqrt{\alpha}$, the curves in Fig. 2(a) vary piecewise without a fixed period. The discontinuity points in Figs. 2(a) and 2(b) correspond to $l = m\pi/\sqrt{\alpha}$, at which the system is unstable and no solitons exist. In both Figs. 2(a) and 2(b), the first branch on the left corresponds to the solutions of the IS. Typical profiles of the IS are given in Figs. 2(c)–2(e). The FW and SH profiles are bell shaped in Figs. 2(c) and 2(e) when α or l_i approaches the left edge of the ISZ branch in Figs. 2(a) and 2(b). The SH in Fig. 2(d) is close to bell shaped except for a small dip in the center when α or l_i approaches the right edge of the ISZ branch.

For a given α and l ($> T_s$), one can calculate l_i and m using $l = l_i + mT_s/2$ and $T_s/2 < l_i < T_s$. The soliton peak of the FWs will appear at $m + 1$ different positions in a sample of length l. Thus, we have $m + 1$ different soliton solutions for one sample. Figure 3 shows a typical case for $l = 66$ and $\alpha = 0.04$. Then one has $T_s = 10\pi = 31.4$, $l_i = 18.88$, and $m = 3$. The soliton peaks appear at four different positions in the sample. The power and width of the FW are the same for all four solutions.

Using the concept of the ISZ, we can construct a family of quadratic solitons consisting of dipole FWs and oscillatory SHs. As shown in Figs. 4(a) and 4(b), the irreducible dipole solitons consist of two monopole ISZs plus one extended zone of width $T_s/2$. The two monopole ISs are exactly identical except for the phase of the FW. There are two types of dipole solitons, the out-of-phase [Fig. 4(a)] and in-phase [Fig. 4(b)] cases, depending on how the phases of the two FW peaks are related. For a given α and $l > 2l_i + T_s/2$, one can calculate l_i and m using $l = 2l_i + T_s/2 + mT_s/2$ with $T_s/2 < l_i < T_s$. The soliton peaks will appear at $2m$ different positions in the sample. Figures 4(c)–4(f) show a typical case for $l = 87$ and $\alpha = 0.04$. Here $T_s = 10\pi = 31.4$, $l_i = 19.95$, and $m = 2$. The two peaks of the FW appear at four different positions in the sample, as shown in Fig. 4, and we have four different in-phase dipole soliton solutions. For the out-of-phase case, one can obtain another eight dipole soliton solutions. All 12 of these solutions are constructed on the basis of one ISZ solution.

In the same way, we can construct a triple soliton solution when the sample size $l > 3l_i + T_s$. The triple solitons have

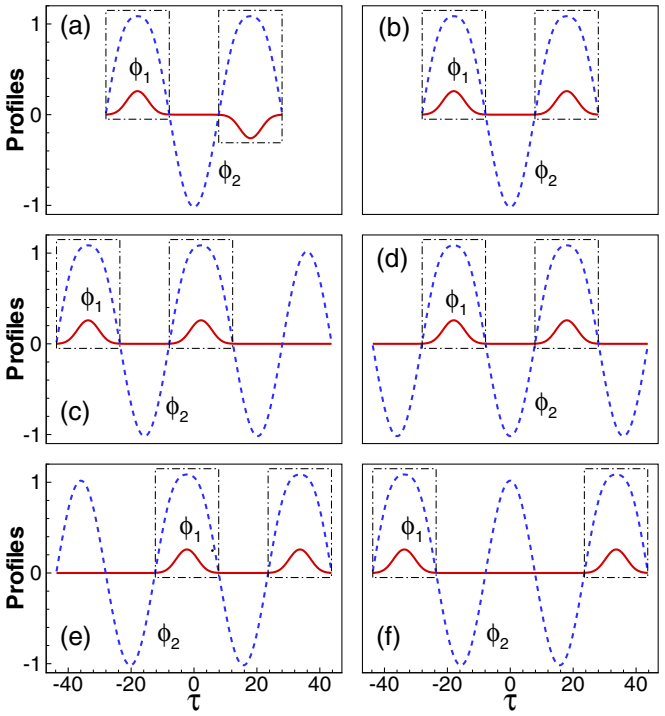

FIG. 4. (Color online) [(a),(b)] Profiles of the irreducible dipole solitons, where $\alpha = 0.04$ and $l = 56$. [(c)–(e)] Profiles of dipole solitons when $\alpha = 0.04$ and $l = 87$. Dash-dotted frames represent the ISZ.

three monopole ISZs plus two extended zone of width $T_s/2$. Generally one can construct a large family of multipole quadratic solitons based on one ISZ solution for a sufficiently large sample.

Our linear stability analysis shows that solitons in the strongly nonlocal case are always stable when subject to boundary confinement. It is noteworthy that the maximum amplitudes of the FWs are much smaller than those of the SHs, and the maximum amplitudes of the SHs in the ISZ are slightly larger than that in the extended zone.

B. Generally nonlocal solutions

In the generally nonlocal case, the oscillatory period T_s for SHs is similar to the soliton width w for FWs. This case is a transition between the strongly nonlocal case ($T_s >> 1$) and weakly nonlocal case ($T_s << 1$). Our numerical results show that it can be regarded as a generally nonlocal case when $1 < \alpha < 4\pi^2$. Figure 5(a) shows typical P and w curves for various α values when $l = 16.84$. The soliton power P increases piecewise and monotonously, and the width w changes piecewise and nonmonotonously with increasing α. Figure 5(b) shows typical curves of the soliton power and width for various l values when $\alpha = 11$ and $T_s = 2\pi/\sqrt{11} = 1.89$. For a given α, the soliton power P and width w for the FWs change piecewise and periodically with a period $T_s/2$ as l increases. In addition, the soliton width w is comparable with the oscillatory period T_s, and the maximum amplitudes of the FWs are always larger than those of the SHs.

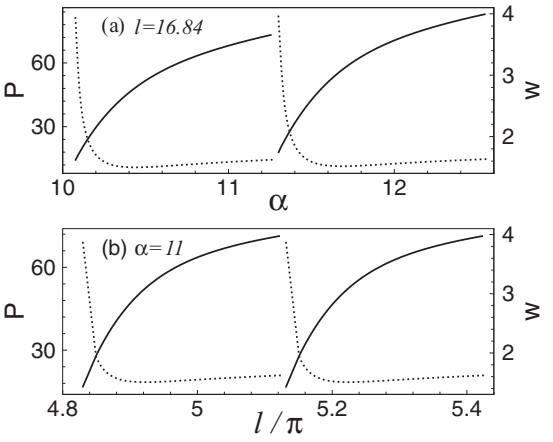

FIG. 5. Soliton power P (solid line) and width w (dotted line) for FW vs the degree of nonlocality α (a) and sample size l (b), respectively.

Two typical soliton profiles are shown in Figs. 6(a) and 6(b). The FW profile in Fig. 6(a) has several shoulder peaks in addition to the central peak, which is similar to the profile of a lattice soliton. The FW profile in Fig. 6(b) is monopole without a shoulder structure. The SH profiles in Figs. 6(a) and 6(b) are both oscillatory. According to the linear stability analysis, solitons in the generally nonlocal case are not always stable. The stability of the quadratic solitons depends

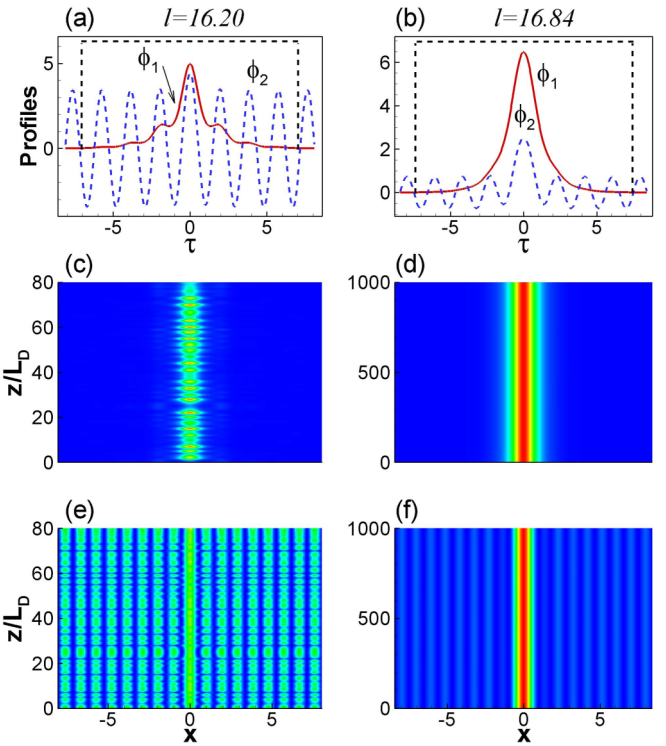

FIG. 6. (Color online) [(a),(b)] Profiles of quadratic solitons for different l when $\alpha = 11$. [(c)–(f)] Simulated propagation of FWs [panels (c) and (d)] and SHs [panels (e) and (f)] corresponding to panels (a) and (b) based on Eqs. (1) and (2). Dash-dotted frames represent the ISZ.

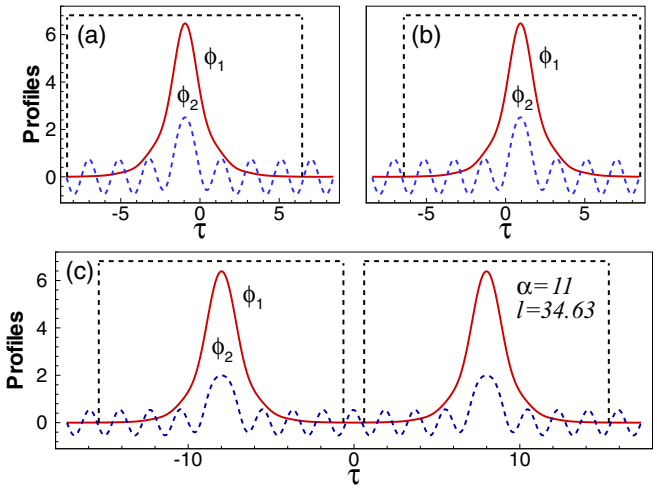

FIG. 7. (Color online) [(a),(b)] Profiles of quadratic solitons for the same l and α as in Fig. 6(b). (c) Typical dipole quadratic soliton profiles with $l_i = 14.95$. Dash-dotted frames represent the ISZ.

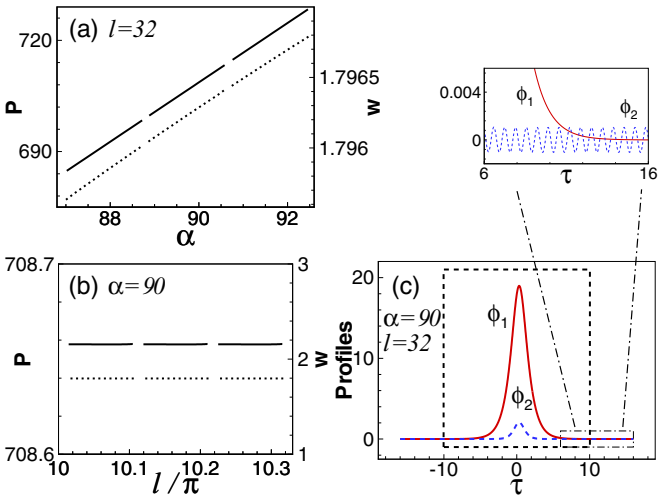

FIG. 8. (Color online) [(a), (b)] Soliton power P (solid line) and width w (dotted line) for FW vs the degree of nonlocality α and sample size l, respectively. (c) Typical soliton profiles with $l_i = 20.08$.

on both α [i.e., $\alpha = (2 + \beta/\lambda)|d_1/d_2|$] and l. Figures 6(c) and 6(e) show unstable propagation of the quadratic soliton, and Figs. 6(d) and 6(f) show stable propagation. The propagation parameters are $d_1 = 1$, $d_2 = -4$, $\lambda = 1$, and $\beta = 42$. Further, we added 3% relative noise as perturbation during propagation.

In the generally nonlocal case, we can also define an ISZ, which includes several SH oscillatory periods, as shown in Figs. 6(a) and 6(b), to cover the entire nonzero FW profiles. Thus, the exact size of the ISZ, l_i, should be determined by numerical solutions, and its value may depend on the numerical accuracy. The numerically obtained typical values of l_i are approximately $5T_s$–$7T_s$ depending on the value of α. When the sample size $l < 5T_s$, the FW profiles will be influenced by the boundary, i.e., $\partial\phi_1/\partial\tau \neq 0$ at the boundary points. When the sample is larger than the ISZ, the entire sample can also be divided into an ISZ and several extended zones. Thus, for a given α and a large l, we have to numerically find the first solution to determine the value of l_i. Then we have the relation $l = l_i + mT_s/2$ and can construct all $m + 1$ solutions for the sample of length l. Figures 6(b), 7(a), and 7(b) show a typical case, where $l = 16.84, \alpha = 11, T_s = 2\pi/\sqrt{11}, l_i = 14.95$, and $m = 2$. The soliton peaks can appear at three different positions in the sample.

When we numerically find that the sample size l is greater than $2l_i + T_s/2$, we can also construct a dipole soliton consisting of dipole FWs and oscillatory SHs, as shown in Fig. 7(c). The irreducible dipole solitons consist of two monopole ISs at each side and one $T_s/2$-wide extended zone in the center. There also exist two types of dipole soliton, which can be in phase or out of phase depending on the relative phase between the two monopole FWs. For a given $l = 2l_i + T_s/2 + mT_s/2$ and α, the peaks of the FWs will appear at $2m$ different positions in the sample. Figure 7(c) shows a typical case, where $l = 34.63, \alpha = 11, T_s = 2\pi/\sqrt{11}$, $l_i = 14.95$, and $m = 4$. The soliton peaks can appear at eight different positions in the sample, and we have 24 solutions for dipole solitons, including in-phase or out-of-phase solitons.

C. Weakly nonlocal solutions

In the weakly nonlocal case, the oscillatory period T_s for SHs is much smaller than the soliton width w for FWs ($T_s << 1$). Our numerical results show that it can be regarded as the weakly nonlocal case when $\alpha > 4\pi^2$. Figure 8(a) shows typical curves of the soliton power and width for various α values when $l = 32$. The soliton power P and width w increase linearly and piecewise with increasing α. Figure 8(b) shows typical P and w curves for various l values when $\alpha = 90$ and $T_s = 2\pi/\sqrt{90}$. For a given α, the soliton power P and width w for FWs remain invariant except for some periodic gaps with a period $T_s/2$ as l increases. Therefore, the power and width of the FWs depend mainly on α, not on the sample size l. A typical soliton profile when $\alpha = 90$ and $l = 32$ is shown in Fig. 8(c). We can see that the maximum amplitude of the FWs is far larger than that of the SHs. The SH profile has a monopole main peak, and the oscillation of the SH continues, although it disappears from view.

In the weakly nonlocal case, we can also define an ISZ, which includes a much longer SH oscillatory period, as shown in Fig. 8(c). Then, for a given α and l, one can determine l_i and $l = l_i + mT_s/2$ numerically, as in the generally nonlocal case. Figures 8(c), 9(a), and 9(b) show a typical case, where $l = 32, \alpha = 90, T_s = 2\pi/\sqrt{90}, l_i = 20.08$, and $m = 18$. Then the soliton peaks can appear at $m + 1$ different positions in the sample of length l.

We can also find solutions of a dipole soliton consisting of dipole FWs and oscillatory SHs, as shown in Fig. 9(c). There also exist two types of dipole solitons, in phase or out of phase solitons. For a given $l = 2l_i + T_s/2 + mT_s/2$ and α, the soliton peaks can appear at $2m$ different positions in the sample. Figure 9(c) shows a typical case, where $l = 64.33$, $\alpha = 90$, $T_s = 2\pi/\sqrt{90}$, $l_i = 20.08$, and $m = 36$. The soliton peaks can appear at 72 different positions in the sample.

Our linear stability analysis shows that solitons in the weakly nonlocal case are always stable when subject to

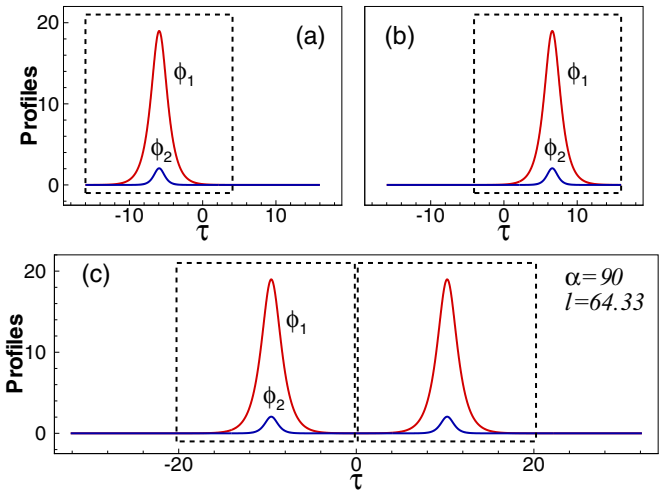

FIG. 9. (Color online) [(a),(b)] Profiles of quadratic solitons for the same l and α as in Fig. 8(c). (c) Typical dipole quadratic soliton profiles with $l_i = 20.08$. Dash-dotted frames represent the ISZ.

boundary confinement. It is noteworthy that the maximum amplitudes of the FWs are much greater than those of the SHs, and the maximum amplitudes of the SHs in the ISZ are also greater than that in the extended zone.

IV. CONCLUSIONS

In summary, we found a family of quadratic solitons subject to boundary confinement. Among them, the FWs are monopole, dipole, or even multipole, and their peaks can appear in any part of the sample. However, the SHs are always oscillatory. Using the concept of the ISZ, we explained the existence of the solitons depending on the degree of nonlocality α and sample size l, for strongly, generally, and weakly nonlocal cases, respectively. In Ref. [27], we found that boundary conditions can stabilize nonlocal solitons, which are the equivalent of quadratic solitons. In this paper, we further showed that the sample size and boundary conditions govern the existence of the solitons. Our results show that boundary conditions play a important role in the propagation and stabilities of nonlocal solitons. This implies that boundary confinement can conquer the singularity and instability in other physical system.

ACKNOWLEDGMENTS

This research was supported by the National Natural Science Foundation of China (Grants No. 11174090 and No. 11174091) and the Scientific Research Foundation of the Department of Education of Guangdong Province (Grant No. 2013CXZDA012).

[1] Yu. S. Kivshar and G. P. Agrawal, *Optical Solitons: From Fibers to Photonic Crystals* (Academic, San Diego, CA, 2003).
[2] A. V. Buryak, P. Di Trapani, D. V. Skryabin, and S. Trillo, Phys. Rep. **370**, 63 (2002).
[3] Yu. N. Karamzin and A. P. Sukhorukov, JETP Lett. **20**, 339 (1974).
[4] Yu. N. Karamzin and A. P. Sukhorukov, Sov. Phys. JETP **41**, 414 (1975).
[5] W. E. Torruellas, Z. Wang, D. J. Hagan, E. W. Van Stryland, G. I. Stegeman, L. Torner, and C. R. Menyuk, Phys. Rev. Lett. **74**, 5036 (1995).
[6] R. Schiek, Y. Baek, and G. I. Stegeman, Phys. Rev. E **53**, 1138 (1996).
[7] W. E. Torruellas, G. Assanto, B. L. Lawrence, R. A. Fuerst, and G. I. Stegeman, Appl. Phys. Lett. **68**, 1449 (1996).
[8] Y. Baek, R. Schiek, G. I. Stegeman, G. Krijnen, I. Baumann, and W. Sohler, Appl. Phys. Lett. **68**, 2055 (1996).
[9] L. Torner and A. Barthélémy, Quantum Electron. **39**, 22 (2003).
[10] G. Assanto and G. I. Stegeman, Opt. Express **10**, 388 (2002).
[11] I. V. Shadrivov and A. A. Zharov, J. Opt. Soc. Am. B **19**, 596 (2002).
[12] M. Mitchell, M. Segev, and D. N. Christodoulides, Phys. Rev. Lett. **80**, 4657 (1998).
[13] W. Hu, T. Zhang, Q. Guo, L. Xuan, and S. Lan, Appl. Phys. Lett. **89**, 071111 (2006).
[14] C. Conti, A. Fratalocchi, M. Peccianti, G. Ruocco, and S. Trillo, Phys. Rev. Lett. **102**, 083902 (2009).
[15] S. Skupin, M. Saffman, and W. Królikowski, Phys. Rev. Lett. **98**, 263902 (2007).
[16] P. Pedri and L. Santos, Phys. Rev. Lett. **95**, 200404 (2005).
[17] Q. Shou, Y. B. Liang, Q. Jiang, Y. J. Zheng, S. Lan, W. Hu, and Q. Guo, Opt. Lett. **34**, 3523 (2009).
[18] N. Ghofraniha, C. Conti, G. Ruocco, and S. Trillo, Phys. Rev. Lett. **99**, 043903 (2007).
[19] X. Gao, J. Wang, L. Zhou, Z. Yang, X. Ma, D. Lu, Q. Guo, and W. Hu, Opt. Lett. **39**, 3760 (2014).
[20] N. I. Nikolov, D. Neshev, O. Bang, and W. Z. Królikowski, Phys. Rev. E **68**, 036614 (2003).
[21] M. Bache, O. Bang, J. Moses, and F. W. Wise, Opt. Lett. **32**, 2490 (2007).
[22] M. Bache, O. Bang, W. Królikowski, J. Moses, and F. W. Wise, Opt. Express **16**, 3273 (2008).
[23] P. V. Larsen, M. P. Sørensen, O. Bang, W. Z. Królikowski, and S. Trillo, Phys. Rev. E **73**, 036614 (2006).
[24] J. Wyller, W. Królikowski, O. Bang, D. E. Petersen, and J. J. Rasmussen, Phys. D **227**, 8 (2007).
[25] A. V. Buryak and Yu. S. Kivshar, Phys. Lett. A **197**, 407 (1995).
[26] B. K. Esbensen, M. Bache, W. Królikowski, and O. Bang, Phys. Rev. A **86**, 023849 (2012).
[27] J. Wang, Y. Li, Q. Guo, and W. Hu, Opt. Lett. **39**, 405 (2014).
[28] M. J. Werner and P. D. Drummond, J. Opt. Soc. Am. B **10**, 2390 (1993).
[29] K. Hayata and M. Koshiba, Phys. Rev. Lett. **71**, 3275 (1993).